

Performance study of the effective gain of the double phase liquid Argon LEM Time Projection Chamber

**C. Cantini^a, L. Epprecht^a, A. Gendotti^a, S. Horikawa^a, L. Periale^a, S. Murphy^a,
G. Natterer^a, C. Regenfus^a, F. Resnati^a, F. Sergiampietri^{a,b}, A. Rubbia^{a*}, T. Viant^a and
S. Wu^a**

^a*ETH Zurich, Institute for Particle Physics,
CH-8093 Zürich, Switzerland*

^b*INFN-Sezione di Pisa
56127 Pisa, Italy*

E-mail: Andre.Rubbia@cern.ch

ABSTRACT: The Large Electron Multipliers (LEMs) are key components of double phase liquid argon TPCs. The drifting charges after being extracted from the liquid are amplified in the LEM positioned half a centimeter above the liquid in pure argon vapor at 87 K. The LEM is characterised by the size of its dielectric rim around the holes, the thickness of the LEM insulator, the diameter of the holes as well as their geometrical layout. The impact of those design parameters on the amplification were checked by testing seven different LEMs with an active area of $10 \times 10 \text{ cm}^2$ in a double phase liquid argon TPC of 21 cm drift. We studied their response in terms of maximal reachable gain and impact on the collected charge uniformity as well as the long-term stability of the gain. We show that we could reach maximal gains of around 150 which corresponds to a signal-to-noise ratio (S/N) of about 800 for a minimal ionising particle (MIP) signal on 3 mm readout strips. We could also conclude that the dielectric surfaces in the vicinity of the LEM holes charge up with different time constants that depend on their design parameters. Our results demonstrate that the LAr LEM TPC is a robust concept that is well-understood and well-suited for operation in ultra-pure cryogenic environments and that can match the goals of future large-scale liquid argon detectors.

KEYWORDS: liquid Argon; Large Electron Multiplier; TPC; double phase; charge extraction; tracking; charging up.

*Corresponding author.

Contents

1. Introduction	1
2. Experimental Setup	2
2.1 The Large Electron Multipliers	4
2.2 Measurement of the effective gain	7
3. Influence of various LEM parameters on the effective gain	7
3.1 Experimental procedure	7
3.2 Gain as a function of the applied electric field	8
3.3 Long term stability and charging up	9
3.4 Uniformity of the gain	13
4. Conclusion	14

1. Introduction

The double phase Liquid Argon Large Electron Multiplier Time Projection Chamber (LAr LEM TPC) is a 3D tracking and calorimetric device which offers many advantages [1, 2, 3]. It has large density, very high granularity, excellent energy resolution and ionisation signal amplification with tuneable gain. Unlike in the case of a single phase LAr TPC [4], where the charge image is readout with wire planes in the liquid, the double phase readout takes advantage of the charge multiplication in gas argon for excellent signal-to-noise ratio on the single signal waveform, yielding optimal image quality over large volumes and low energy threshold. The amplification of the drifting charges in gas allows to build LAr TPCs to large scales and low threshold that are required by future long baseline neutrino experiments. In this context, the Giant Liquid Argon Charge Imaging Experiment (GLACIER [5, 6, 7]) is proposed as far detector for the future European Long Baseline Neutrino Experiment (LBNO [8]), enabling measurements over a wide range of energies from the MeV to multi-GeV and addressing a broad spectrum of fundamental physics topics, including long-baseline neutrino oscillations, proton decay search and supernova and atmospheric neutrinos detection. A large-scale demonstrator is being currently planned in the context of the LBNO-DEMO (CERN WA105) experiment [9].

In the double phase LAr LEM TPC, the ionisation charge is extracted to the Argon vapour, where it is amplified by a LEM stage, which triggers Townsend multiplication in the high electric field regions in the LEM holes [10]. See Figure 1. After their long drift within the liquid phase with a drift field of typically 0.5 kV/cm, ionisation electrons are efficiently extracted from the liquid with an electric field of around 2 kV/cm and amplified with a field of about 30 kV/cm applied across both electrodes of the LEM. The amplified charge is then collected and recorded on

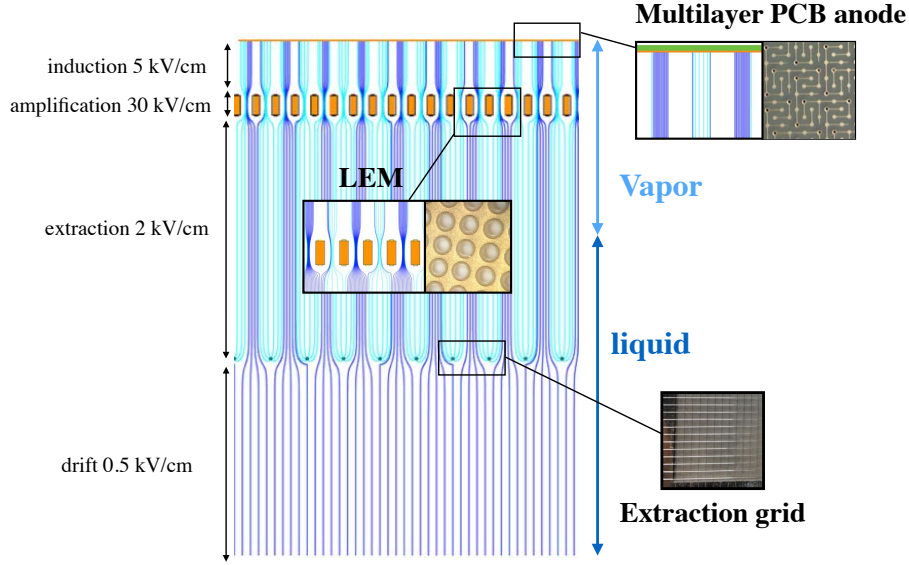


Figure 1. Illustration of the amplification region in a double phase LAr TPC. The simulated field lines in dark blue are an indication of those followed by the drifting charges (without diffusion).

a two-dimensional and segmented anode. The anode consists of a set of strips (views) that provide the x and y coordinate of the event with a mm-level granularity.

The double phase principle was repeatedly successfully demonstrated on a chamber equipped with a $10 \times 10 \text{ cm}^2$ area readout (see e.g. Refs. [1, 11]) and on a larger device consisting of a $40 \times 80 \text{ cm}^2$ readout and 60 cm drift [12]. We were able to operate both setups in a stable condition at constant gains of about 15 corresponding to $S/N \approx 60$ for MIPs. The possibility of obtaining such large signal-to-noise ratios is very appealing, considering the fact that increasing detector sizes with longer drifts and larger readout capacitances lead to a degradation of the imaging quality of the device. Future large double phase TPCs will be composed of anode and LEM modules of $50 \times 50 \text{ cm}^2$ area. In Ref. [13] we demonstrated that for large areas the electronic noise could be kept within ~ 1000 electrons for a two meter readout by using an innovative design of multilayer PCB anodes.

In this paper we study in more detail the effective gain and investigate in which manner the design specifications of the LEM affect the amplification of the drifting charges. The relevant features of the LEM are 1) the diameter of the hole, 2) the thickness of the insulator, 3) the size of the dielectric rim around the holes and 4) the geometrical arrangement of the holes. The LEM parameters potentially affect the effective gain of the chamber either by changing the electric field configuration inside the LEM hole or modifying the electrical transparency of the system.

2. Experimental Setup

The LEMs are tested in the so-called “3 liter” setup which is a double phase LAr LEM TPC consisting of a 21 cm long drift length and a $10 \times 10 \text{ cm}^2$ area. The setup has now been operated for more than 4 years, it is a well understood detector and very useful for testing new ideas with a

rapid turn-around. A description of the apparatus can be found in Ref. [13]. In Figure 2 we show a picture of the drift cage along with photos detailing the charge readout system.

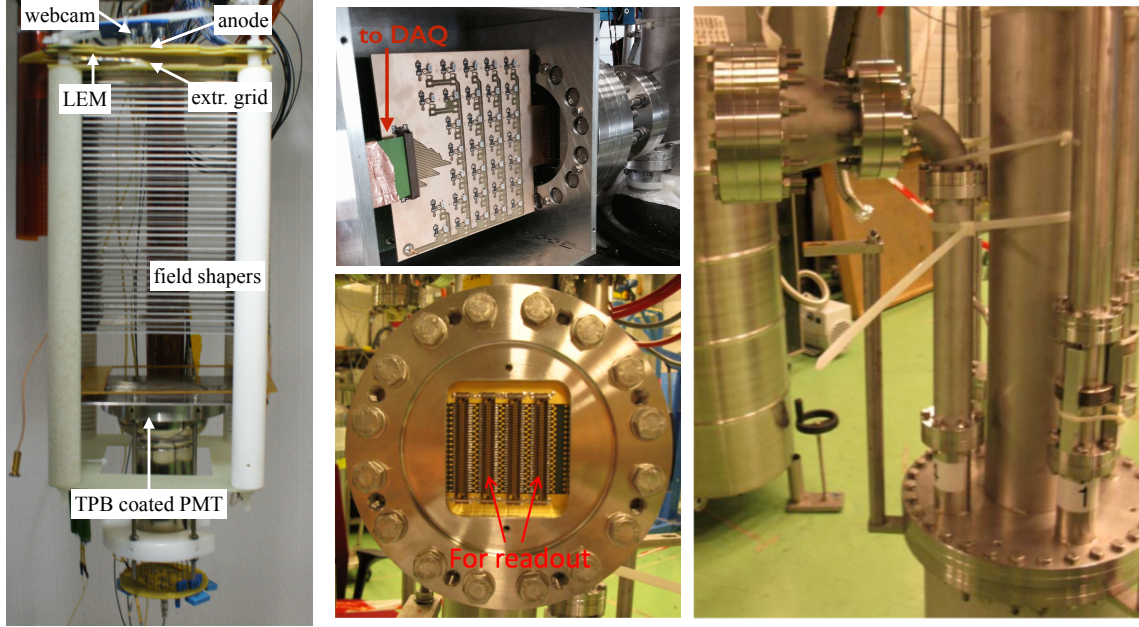


Figure 2. Picture of the 3 liter TPC (left) and of the stainless steel chimney through which the signal cables are brought outside of the cryostat to the decoupling boards and to the DAQ.

The free charges from the ionisation are drifted towards the LAr surface driven by a constant drift field of 500 V/cm. A larger electric field of about 2 kV/cm is applied at the vicinity of the LAr surface to efficiently extract the drifting charges to the vapour phase. The extraction field is confined in a 10 mm region between the LEM and a stainless steel grid placed in the liquid. The grid consists of 100 μm stainless steel wires tensed and positioned at a constant pitch of 3 mm in both x and y direction matching the anode strips. This configuration guarantees that close to 100 % of the drifting charges are extracted and focussed towards the LEM holes. The amplification and readout of the charge is then performed by the LEM and anode. An electric field of at least 30 kV/cm is applied across the LEM in order to obtain charge amplification in the dense pure argon vapour. The electrons are collected on the anode placed 2 mm above the LEM.

In view of larger scale operation we tested a configuration whereby the high voltage decoupling of the readout and discharge protection system are all mounted on two dedicated PCBs placed immediately outside of the chamber. In this configuration the 64 signal cables are routed out via two twisted pair cables of 32 channels through a stainless steel chimney that is terminated with an ultra-high vacuum leak-tight feedthrough. Pictures are shown in Figure 2-right. The flange is actually made of a Stainless Steel ring, in which a several mm-thick multilayer PCB is sealed. The multilayer PCB is designed in order to accommodate connectors on both faces. We believe this system to be scalable to flanges of larger diameters that can accommodate a higher number of channels as developed in Ref. [9]. The signals are then amplified and digitised by the specially developed CAEN SY2791 readout system (see Ref. [12]).

Before operation the liquid level is precisely adjusted between the extraction grid and the

LEM by monitoring the capacitance between both systems. During filling for the first time were able to visually inspect the rise of the liquid argon level by installing a webcam combined with LED lighting above the anode. The webcam is a Microsoft VX-1000 described in Ref. [14]. It produces a clear image of the level during the filling. However once the chamber is filled and the camera reaches the temperature of argon vapour, the image is no longer visible. The camera becomes operational again once at room temperature. For future operations of large tanks we envisage to embed the camera in a dedicated casing with heaters to ensure a constant visual monitoring.

In order to keep the chamber at liquid argon temperature, it is fully immersed in an open bath filled with liquid argon. In these conditions the chamber is operated at a stable pressure of around 980 mbar slightly above the atmospheric pressure in our lab of 960 mbar. The detector is however subject to slight pressure variations resulting from external modifications from the weather conditions. In addition the pressure rises periodically when the level of the open bath decreases below the top flange of the detector before it is re-filled by an operator. These pressure variations affect the operations of the chamber and will be corrected for as described later.

2.1 The Large Electron Multipliers

The Large Electron Multipliers (LEM) consist of copper cladded epoxy plates with a thickness of a millimeter and with mechanically drilled holes. The holes have diameters of $500\text{ }\mu\text{m}$ and there are order of 200 holes per cm^2 . Applying a sufficient potential difference to the two metal faces of about 30 kV/cm , an electric field strong enough to trigger the Townsend avalanche is attained in the holes. The photons produced during the avalanche are absorbed by the dielectric walls of the holes, ensuring the confinement of the multiplication in absence of quenching gases. The LEM is also well suited for the operation in cryogenic conditions because the thermal expansion coefficient of the metal and of the glass epoxy are well matched. It sustains without any damage abrupt cooling down and warming up cycles, and is a device known to be resistant to discharges. The $10\times 10\text{ cm}^2$ LEMs used for our measurement are produced at a PCB manufacturing company called ELTOS¹. Pictures of some samples are shown in Figure 3. About 15'000 holes are mechanically drilled with standard PCB techniques in the copper cladded glass epoxy plate. In order to reduce the probability of discharge at the edge of the holes, a dielectric rim is produced by etching away the copper around the periphery of these latter. In order to guarantee uniform sizes and perfect entering, the rims are produced by a mask-less etching technique developed at CERN [15]. The rims are typically a few tens of micrometer large, their size is limited by the initial thickness of copper. The metallisation of the LEM extends about one centimeter around the area with the holes in order to properly shape the electric field at the edge of the chamber active area.

The parameters that characterise the LEMs are the hole diameter, the thickness of the epoxy plate, the geometrical arrangement of the holes and the size of the rim. The complete list of the LEMs we tested along with their individual specifications are provided in Table 1. The precision on the parameters are those quoted by the company and verified independently by us on some samples.

The multiplication of the electrons in the LEM holes depends on the electric field created by applying a voltage V across the LEM of thickness d . We present our results as a function of the effective electric field $E_0 = V/d$, in reality the field inside the hole is always weaker than

¹www.eltos.it

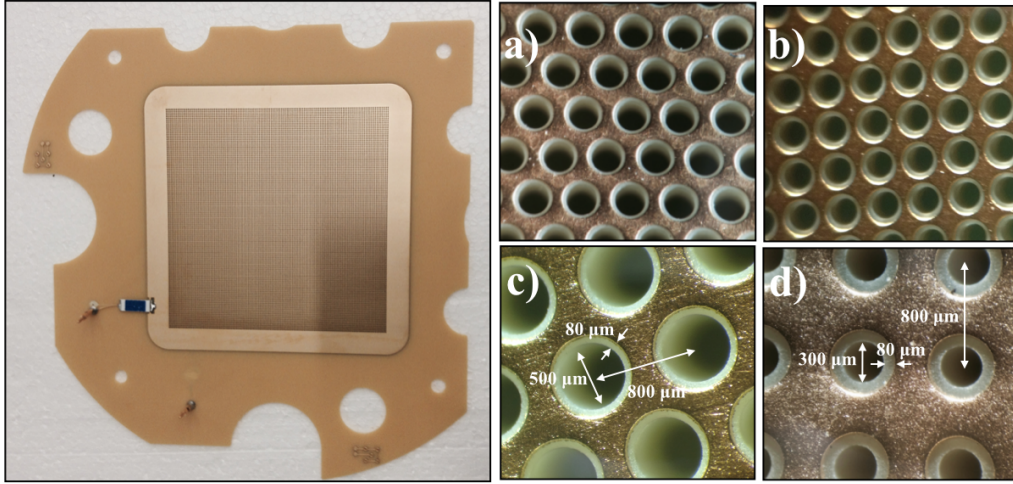


Figure 3. Left: picture of one of the $10 \times 10 \text{ cm}^2$ LEMs we tested in our chamber. A microscope view of some LEM samples is shown on the right: the hexagonal hole arrangement (a) is compared to the square arrangement (b) and on the bottom zooms (c) and (d) on two samples with different hole sizes are shown.

		precision	LEM1	LEM2	LEM3	LEM4	LEM5	LEM6	LEM7
rim size (μm)		± 3	80	80	40	80	40	80	80
FR4 thickness (mm)		$^{+0}_{-0.06}$	0.8	1	1	1	1	1	0.6
copper thickness (μm)		± 5	80	80	40	80	40	80	80
hole diameter (μm)		$^{+0}_{-25}$	500	500	500	400	500	300	500
hole layout (μm)		-	square	square	hexagonal	square	square	square	square
number of holes		-	15084	15084	16761	15084	15084	15084	15084
κ (see text)		-	0.789	0.830	0.900	0.905	0.900	0.938	0.699
measured capacitance (pF)		± 10	539	450	479	500	531	557	560

Table 1. Specifications of the LEMs tested in our setup.

the nominal E_0 . The computation of the field along the hole axis shown in graph a) of Figure 4 indicates that the field is larger at the center of the hole. However, as shown in graph b), the field is even greater on the side of the holes close to the insulator. The charge multiplied in the center region of the hole is efficiently transferred to the anode, while the one produced in the side region is more prone to be collected on the top electrode. Therefore the larger field on the hole edges may be responsible for discharges without significantly contributing to the amplification.

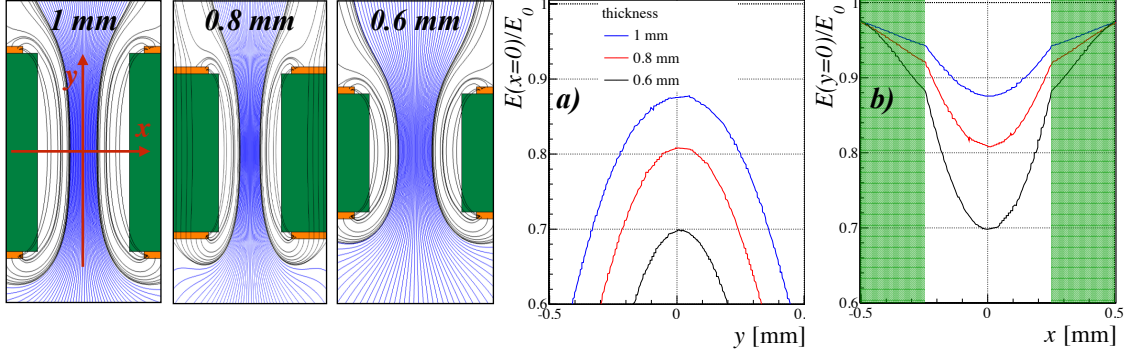


Figure 4. Computation of the electric field lines inside a LEM hole for three different thickness of the insulator indicated on the figure (all the LEMs have a rim $80 \mu\text{m}$ and a hole diameter of $500 \mu\text{m}$). The field lines followed by the drifting charges are shown in blue. The two graphs, *a*) and *b*), show the ratio of the norm of the electric field at the center of the hole ($x=0$, resp. $y=0$) to the field applied across the electrodes (E_0) as a function of the y (resp. x) coordinates. The shaded green area delimits the hole edges.

We define κ as the ratio of the field at the center of the hole ($x=0, y=0$) to the applied field E_0 and $E \equiv \kappa E_0$ as the amplification field. The effective gain G_{eff} of the LEM is then generally expressed with the function [3]:

$$G_{eff}(E, \rho, t) \equiv \mathcal{T} e^{\alpha(\rho, E)x} \times \mathcal{C}(t) \quad (2.1)$$

where \mathcal{T} is a parameter proportional to the electrical transparency of the chamber; $\alpha(\rho, E)$ is the first Townsend ionisation coefficient for the amplification field E and density ρ ; x denotes the effective amplification length which can be geometrically related to the length of the field plateau along the hole axis shown in graph *b*) of Figure 4; and $\mathcal{C}(t)$ represents any time variation of the gain. The generalised form of the first Townsend coefficient as a function of the medium density ρ and the electric field E can be approximated by [16]:

$$\alpha(\rho, E) = A\rho e^{-B\rho/E} \quad (2.2)$$

where A and B are parameters depending on the gas. A fit to the electric field dependence of the Townsend coefficient in the range between 20 and 100 kV/cm predicted by MAGBOLTZ [17] calculations, gives $A\rho = (7339 \pm 90) \text{ cm}^{-1}$ and $B\rho = (183 \pm 1.0) \text{ kV/cm}$ for pure argon at 87 K and 0.980 bar. We refer the reader to Ref. [18] for a detailed explanation of charge amplification inside the LEM hole.

The results from electrostatic simulations presented in Figure 4 indicate that both the amplification field and length increase with thicker LEMs. The same simulations show that they also increase with smaller rim sizes and smaller hole diameters. However those simulations do not take into account parameters that affect the effective gain such as, for instance, the electrical transparencies and breakdown voltages of the LEMs. The results from the data presented in the next sections fully characterises the LEMs in terms of their maximal effective gain as well as time evolution of the effective gain in pure Argon at 87 K.

2.2 Measurement of the effective gain

The 3L chamber was exposed to large samples of cosmic muons tracks which were used to characterise the response of the chamber in terms of effective gain, signal-to-noise ratio and energy resolution. The analysis (noise filtering, hit-finding, track reconstruction etc..) of all the data is performed with the QScan software package [19, 20]. The reconstruction method is similar to that described in Ref. [12] and includes also an algorithm that searches for residual hits which are interpreted as δ -rays a of few MeV emitted by the traversing ionising particles. The crossing muons, once reconstructed in 3D, allow us to retrieve the length of the track on each strip of view 0 and view 1 (Δs_0 and Δs_1), along with the charge collected on the corresponding channels (corrected for the electron lifetime), ΔQ_0 and ΔQ_1 . The charge collected by unit length $\Delta Q_0/\Delta s_0$ and $\Delta Q_1/\Delta s_1$, which are proportional to the energy locally deposited by the track in liquid Argon, are the relevant quantities used to evaluate the performance of the LEM and estimate the gain of the chamber. Since the cosmic muons that cross the chamber are minimum ionising particles the average charge deposition along a track, predicted by the Bethe-Bloch formula and accounting for electron-ion recombination [21] is $\langle \Delta Q/\Delta s \rangle_{MIP} = 10$ fC/cm. By using the sum of the collected charge per unit length on both views we hence define the measured effective gain by:

$$G_{eff} = \frac{\langle \Delta Q_0/\Delta s_0 \rangle + \langle \Delta Q_1/\Delta s_1 \rangle}{\langle \Delta Q/\Delta s \rangle_{MIP}} \quad (2.3)$$

G_{eff} takes into account the charge multiplication in the LEM holes, as well as potential charge reduction from the liquid-vapour extraction efficiency and from the transparency of the grid and the LEM.

3. Influence of various LEM parameters on the effective gain

3.1 Experimental procedure

Before installation the LEM is washed with high-pressure deionised water and further cleaned in an ultrasonic bath filled with pure alcohol. In order to test the absence of resistive contacts between two electrodes, the LEM is powered in air. Typical fields of about 35-40 kV/cm should be reached and the measured leakage current should not exceed 10 nA. The voltage is then increased further until discharges occur, their location are monitored to be sure that there is no particular region more susceptible to spark. The controlled sparks train the LEM since they remove dust and burn the fibers inside the hole.

The LEM is then mounted on the chamber and the high voltage is supplied to the two electrodes through metal pins (see Figure 3). The 500 M Ω resistor between the high voltage connector and the electrode acts a spark protection device by limiting the current across the hole during the discharge. Before filling with liquid argon, the main vessel containing the chamber is first evacuated to residual pressure below 5×10^{-6} mbar and filled with pure liquid Argon trough an activated copper and zeolite powder cartridge. The level of the liquid is precisely adjusted in-between the extraction grid and LEM by monitoring the capacitance of the LEM-grid system. The webcam provides complimentary visual check of the liquid level. The liquid Argon purity is monitored throughout the data taking period by measuring the lifetime of the drifting electrons. The purity is typically

below 1 part per billion (ppb) after filling and decreases at a rate of about 1.4 ppb per day mainly due to the outgassing of material in the relatively small gas volume of the chamber.

The seven LEMs listed in Table 1 were tested in seven independent runs with the same experimental procedure. We first performed electric field scans of the LEM: at each field setting across the LEM cosmic data was acquired for ~ 15 minutes at a rate of about 5 Hz. The field was ramped up by steps of 1 kV/cm until the breakdown voltage was reached. For each LEM setting the induction and extraction fields were always adjusted at the nominal values of 5 kV/cm and 2 kV/cm in the liquid respectively. The electric field scan was the first data-set to be recorded after the chamber is filled, meaning that the LEM was polarised for the first time during the scan. Once the scan was finished we acquired data continuously for a period of a few days at constant electric field settings. The chamber was then emptied, opened to air and the next LEM was mounted. The only differences between the runs were the LEMs and the fields at which they were operated. In the next two sub-sections the results of the electric scans and the longer-term operation are discussed.

3.2 Gain as a function of the applied electric field

In this section we compare the results of electric field scans obtained on all the LEMs. The results are presented in Figure 5 where the effective gain is plotted as a function of the applied electric field across the LEM electrodes (E_0). The results are grouped together in such a way that the only difference between the LEMs is the parameter indicated in the legend. The effective gain is corrected for the electron lifetime and normalised to a pressure of 980 mbar. The data points are fitted with the function described in Equation 2.1. Since the LEM field scans occur on a short timescale of typically 2 hours we can neglect time variations of the gain $\mathcal{G}(t)$ during this period. This point will be justified in the next section. As can be seen, for all the LEMs the measured effective gains exhibit the expected exponential dependence with the LEM field. During the fit κ was fixed at the values from the electrostatic field simulation results and \mathcal{T} together with the amplification length, x , were left as free parameters. For all measurements the maximum reachable gain was always limited by the occurrence of discharges. The highest electric field setting at which data could be stably recorded is defined as E_0^{\max} and the corresponding gain as G_{eff}^{\max} . The results are summarised in Table 2 and are discussed below:

- (i) *Impact of the hole geometrical layout*: the electrical transparency is significantly higher for the LEM with the hexagonal hole layout. They also have near identical amplification lengths. This can be understood graphically from the fact that both curves remain parallel. Since both LEMs breakdown at the same electric field the one with the hexagonal hole layout has a significantly larger G_{eff}^{\max} of almost 200.
- (ii) *Impact of the hole diameter*: electrostatic simulations predict a slightly larger amplification length as the hole sizes decreases. We indeed observe this phenomena which translates into a faster rise of the effective gain with the electric field. We also notice that, due to the increased amplification field, at a given E_0 the gain is larger for the LEMs with smaller holes. However the results from the fit also indicate that the electrical transparency of the LEM reduces with smaller holes. We do not observe any improvement of the LEM performance in terms of maximal gain. All three LEMs are able to reach gains of about 120.

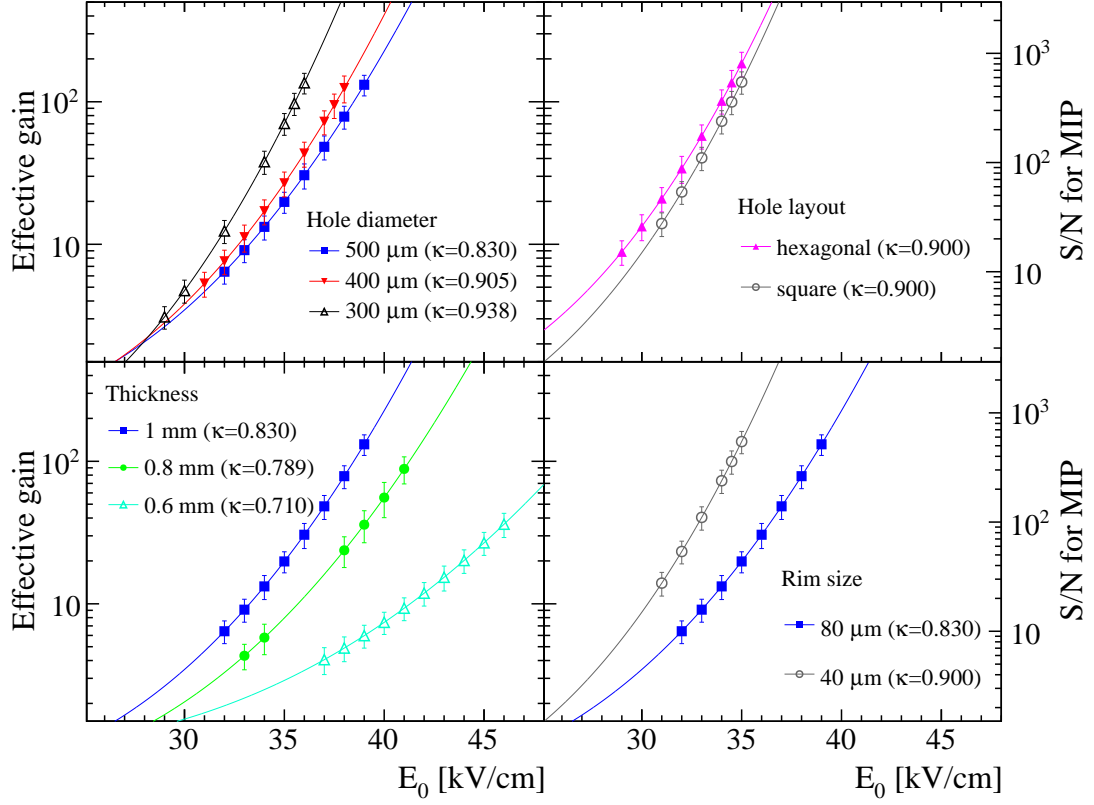


Figure 5. Comparison of effective gains for various LEMs in pure argon vapor at 87 K as a function of the electric field applied across the electrodes. The data points are fitted with the function described in the text.

- (iii) *Impact of the thickness:* we see a clear enhancement of the slope for thicker LEMs due to the increase of the amplification lengths. We also observe that the maximal reachable gains are significantly lower for thinner LEMs.
- (iv) *Impact of the rim size:* we qualitatively observe an increase of the amplification length with the LEM of smaller rim size. However although not shown on the Figure, we observed from previous data that the maximal reachable gain was typically a factor two lower if we do not etch a rim around the LEM holes. The importance of the rim although in other gases and temperatures is discussed e.g in Ref. [15]. Based on these results we do not see a benefit of going to a larger than 40 μm rims. On the contrary since for larger rims the amplification field is lower we need to apply higher voltages across the LEM to reach comparable gains.

3.3 Long term stability and charging up

Immediately after finishing the LEM scans, the chamber was operated at fixed electric field settings for at least one day to study the gain evolution over time. The LEM fields were polarised according to the values from Table 3. For all LEMs, their initial gain at t_0 were found to decrease and then stabilise after a typical time of half a day as shown in Figure 6. The effective gain at t_0 , defined

tested parameter	value	LEM	\mathcal{T}	x (mm)	G_{eff}^{max}	E_0^{max} (kV/cm)
hole layout	hexagonal	3	0.59 ± 0.18	0.96 ± 0.07	182	35
	square	5	0.34 ± 0.14	0.94 ± 0.08	123	35
hole diameter	500 μm	2	0.46 ± 0.14	0.73 ± 0.05	124	39
	400 μm	4	0.41 ± 0.11	0.81 ± 0.05	124	38
	300 μm	6	0.20 ± 0.03	0.88 ± 0.04	134	36
thickness	1 mm	2	0.46 ± 0.14	0.73 ± 0.05	124	39
	0.8 mm	1	0.46 ± 0.15	0.69 ± 0.06	88	41
	0.6 mm	7	0.58 ± 0.2	0.55 ± 0.06	36	46
rim size	40 μm	5	0.34 ± 0.14	0.94 ± 0.08	123	35
	80 μm	2	0.46 ± 0.14	0.73 ± 0.05	124	39

Table 2. summary of the results retrieved from the LEM electric field scans. The definitions of the variables are given in the text.

as G_{eff}^0 , is from the data taken during the LEM electric field scan at the corresponding electric field. All the data points are corrected for pressure variations and normalised to a fixed pressure of 980 mbar in order to have a direct comparison. We observe that the effective gain $G_{eff}(t)$ relaxes from an initial gain of G_{eff}^0 to a stable value, G_{eff}^∞ , after a characteristic time τ . The time evolution of $G_{eff}(t)$ can be empirically described as:

$$G_{eff}(t) = \frac{G_{eff}^\infty}{1 - \left(1 - \frac{G_{eff}^\infty}{G_{eff}^0}\right) \times e^{-t/\tau}} \quad (3.1)$$

This phenomenon was already observed and described in one of our previous publications [13] and is understood to be a consequence of the charge accumulation on the insulator inside and around the hole. A simulation of this effect along with the impact on the gain is given in Ref. [22]. During these long term operations, occasional discharges occurred between the top and bottom electrodes of the LEM. These discharges do not affect the evolution of the overall gain of the LEM.

Table 3 summarises the total data taking and the number of discharges recorded by the power supply for all the LEMs. As none or very few discharges occurred during typical run times of several tens of hours, we regard the LEM as a very stable apparatus operating at a stable effective gain of around 20. For the purpose of these measurements data taking was stopped after periods of a few days. We have already shown in [13] that, once charged up, the LEM can be operated at the stable gain, G_{eff}^∞ , with very few discharges for periods of at least one month. The gain remains stable unless the run is stopped and the chamber is exposed to air which neutralises the charges stuck to the dielectric of the LEM.

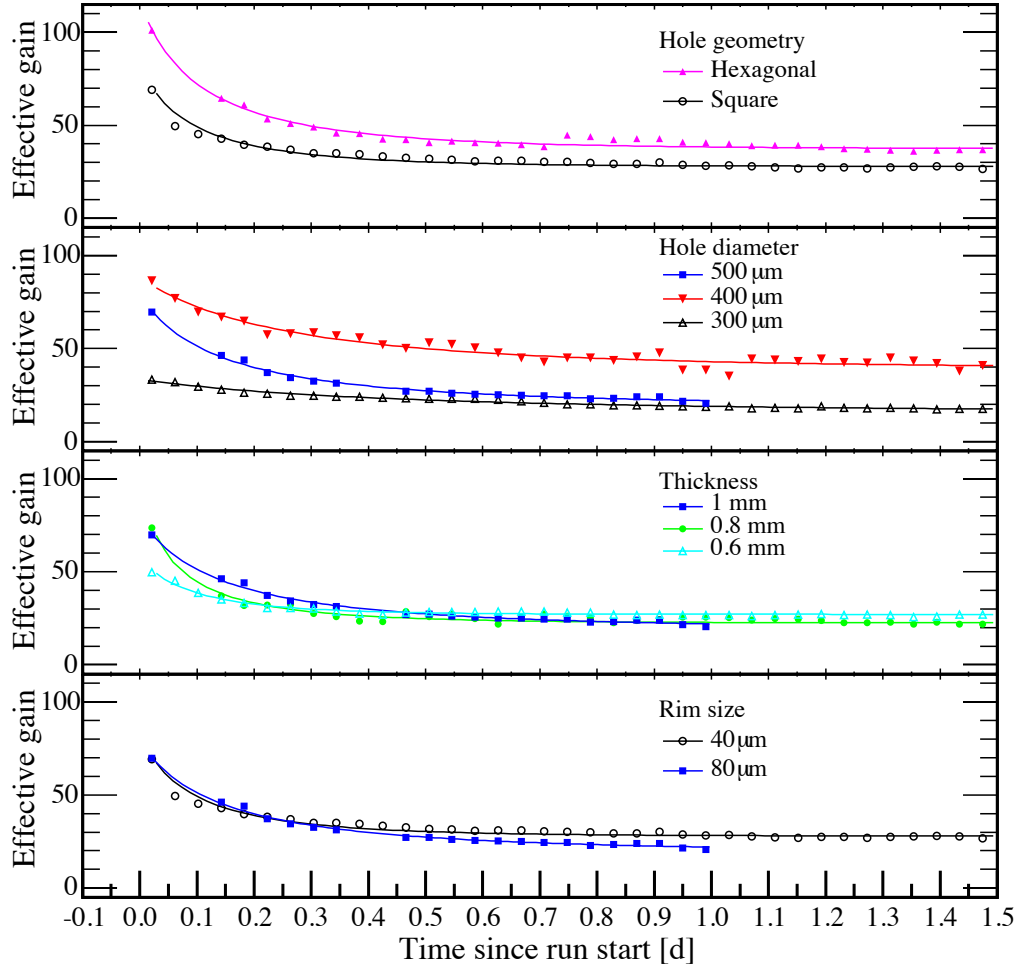


Figure 6. Comparison of the time evolution of the effective gains for various LEMs in pure argon vapor at 87 K. The data points are fitted with the function described in the text.

Since we compare LEMs operated at different effective gains we also studied the response of the same LEM (LEM 3) operated at three different electric fields in three independent runs. The results are shown in Figure 7. From these measurements we conclude that 1) if the initial gain or applied electric field is larger the LEM will charge up faster and 2) the ratio between the initial gain and final gain is independent of the field at which the LEM is operated.

The impact from the different LEM parameters on the charging-up time τ as well as the ratio between initial and final gain have been investigated and are summarised in Table 3. They are discussed separately in the following paragraphs:

- (i) *Impact of the hole geometrical layout:* both LEMs were operated at the same E_0 but, because of their different electrical transparencies (see Section 3.2), the LEM with the hexagonal hole

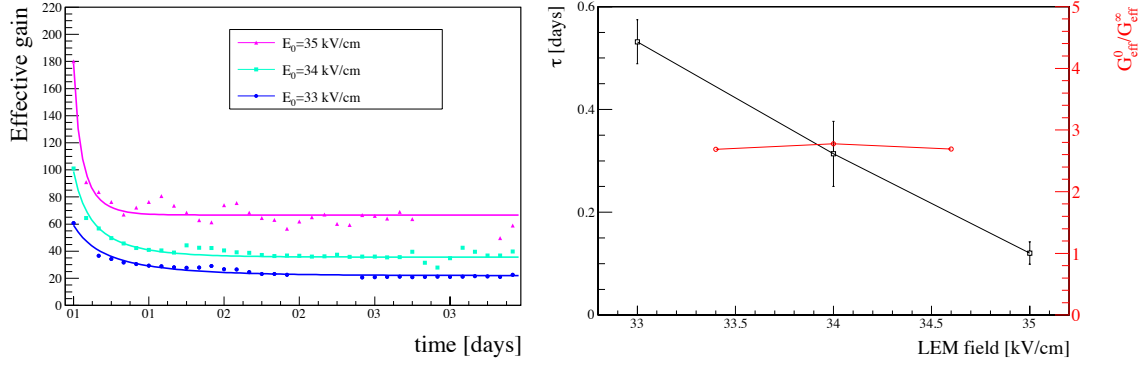


Figure 7. Left: evolution of the effective gain for the same LEM (LEM 3) operated in three independent runs with different electric field settings. Right: value of τ and the ratio of the initial to stable gain as a function of the applied electric field.

layout has a much larger initial gain. Since we observe identical charging-up time constants we remark that the evolution of τ observed in Figure 7 may be an effect of the applied electric field rather than the initial effective gain. We also notice that the hole layout has no impact on the ratio between initial and final gain.

- (ii) *Impact of the hole diameter:* although operated at different electric fields the runs with LEMs of three different hole diameters have a similar stabilisation time around 0.5 days. The ratio between the initial and final gain tend to decreases as the hole diameter becomes smaller. More discharges were observed during the runs with LEMs of smaller diameter holes compared to any other runs. This is especially true for the 300 μm hole LEM which was operated at a relatively low gain for a duration which is comparable to other runs. One possible explanation is that smaller holes are more difficult to clean. Another explanation is that, in smaller diameter holes, the electrons from the avalanche are more susceptible to reach the edge of the hole where the electric field is larger and thus produce a discharge (see Section 2.1).
- (iii) *Impact of thickness:* a reduction of the LEM thickness clearly results in a smaller ratio between the initial and final gain and a faster stabilisation time. As indicated in Figure 7 the faster charging-up time could be an effect of the larger electric field needed to polarise thinner LEMs. The reduction of the ratios, $\frac{G_{eff}^0}{G_{eff}^\infty}$, are evidence that the gain of the LEM evolves to a stable value because of free charges sticking inside the holes. As observed in Section 3.2, thinner LEMs cannot reach very high gains because of their shorter amplification lengths. On the other hand they have the advantage of relaxing faster and stabilising at relatively larger gains.
- (iv) *Impact of the rim size:* both LEMs were operated at similar initial gains and we clearly observe that the LEM with the smaller rim has a faster stabilisation time and a larger ratio between initial and final gain. Studies at different gas and temperature conditions [15, 23] showed similar conclusions: wider rim result in longer stabilisation time and larger ratios between initial and final gain. One possible explanation is that the exposed di-electric material increases with the rim size providing a larger area around the hole for free charges to stick.

Parameter	Value	LEM	E_0 [kV/cm]	Run-time [hrs]	No. of discharges	τ [days]	G_{eff}^0	G_{eff}^∞	$\frac{G_{eff}^0}{G_{eff}^\infty}$
geometry	hexagonal	3	34	110	0	0.32 ± 0.07	99	35	2.7
	square	5	34	52	0	0.30 ± 0.02	65	27	2.4
hole	500 μm	2	38	24	0	0.53 ± 0.05	70	20	3.5
	400 μm	4	37	50	2	0.53 ± 0.07	84	40	2.1
	300 μm	6	33.5	75	3	0.75 ± 0.04	32	16	2.0
thickness	1 mm	2	38	24	0	0.53 ± 0.05	70	20	3.5
	0.8 mm	1	42	82	0	0.24 ± 0.02	73	22	3.3
	0.6 mm	7	46	95	1	0.18 ± 0.01	51	27	1.9
rim size	80 μm	2	38	24	0	0.53 ± 0.05	70	20	3.5
	40 μm	5	34	52	0	0.29 ± 0.02	65	27	2.4

Table 3. Summary of the results obtained from the longer term stability runs. The definitions of the variables are given in the text.

3.4 Uniformity of the gain

In addition to the effective gain, we also studied if the hole layout impacts the uniformity of the charge sharing between both views. Figure 8 shows the alignment between the extraction grid, the LEM holes and the anode strips. The LEM square and hexagonal hole layouts are compared: on the former the holes are aligned with the pads of the anode readout strips whereas in the hexagonal layout there is no specific matching between the holes and the anode pattern. In both cases the extraction grid wires are precisely aligned between the anode readout strips. Since the LEM with

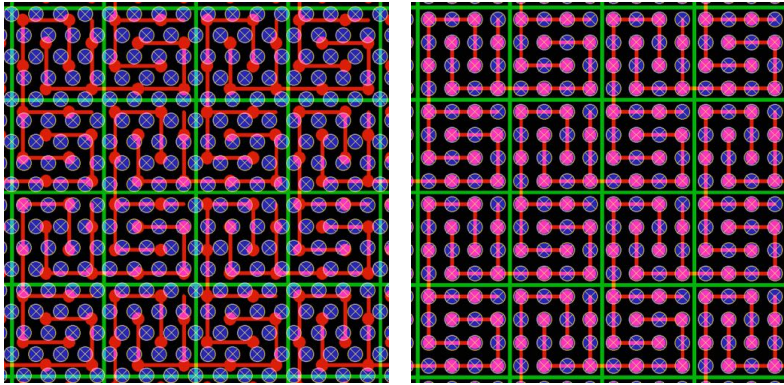


Figure 8. Schematic of the matching between the extraction grid (green lines) the LEM holes (in opaque blue) and the multilayer PCB anode copper tracks (red pattern). In the case of the square LEM hole arrangement (right) the holes are aligned to the anode copper tracks.

the hexagonal hole layout is the most transparent to drifting electrons and offers some of the best

performances in terms of maximal achievable gain it is important to check that the hole layout does not degrade the imaging capabilities of the chamber. This could occur either by introducing large channel-to-channel fluctuations of the gain or compromising the symmetry of the charge sharing between both views.

In Figure 9 we compare the gain measured on each strip along the x and y coordinates (or equivalently view 0 and view 1) for both hole layouts. In both cases, a strip-to-strip fluctuation is

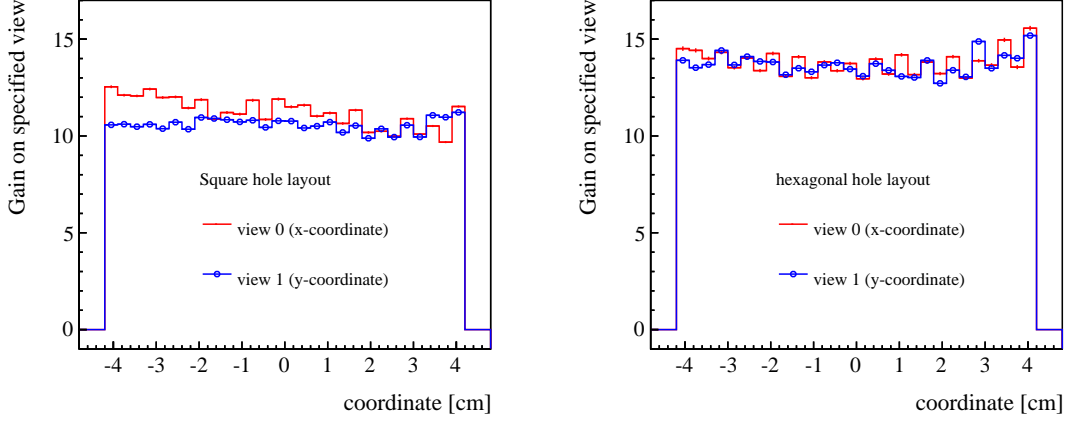


Figure 9. Projections of the measured gains along both views in the case of the LEM with the square (left) and hexagonal (right) hole layout)

seen which is partly due to the limited precision on the alignment between the extraction grid and anode strips. The slight smooth trend on top of the strip-to-strip fluctuations is a consequence of variations in the LEM thickness. Even if, for future operations of larger detectors, this effect of the LEM thickness can be calibrated it will be important to precisely measure the thickness of the LEM insulator.

In both cases, a deviation of within $\pm 10\%$ from the mean is achieved for all the strips in both coordinates. Taking into account also the variation in the electronics sensitivity which are typically of $\pm 5\%$ from channel to channel, the $\pm 10\%$ variation is within an acceptable region. For the square hole layout, we observed a 5% difference in the charge collected by two views. This is due to the limited precision to match the anode pads with the LEM holes. For the hexagonal hole layout, the charge sharing between two views is within 1% due to the random matching between the anode and LEM hole which smears out the difference. We can therefore conclude that no bias is introduced by using LEMs with hexagonal hole layouts.

4. Conclusion

We have compared the response of LEMs with different characteristics in pure argon vapor at 87 K. In seven separate runs on a LAr LEM TPC of $10 \times 10 \text{ cm}^2$ active area we have checked the impact of the rim size, hole diameter, insulator thickness and hole arrangement on both the maximal initial gain and its long term evolution. Each LEM has a different response; the maximal achievable gain

was 180 corresponding to $S/N \approx 800$ for MIPs over a 3 mm readout pitch. This impressive S/N was obtained with a LEM of 1 mm thickness, 40 μm rims and 500 μm diameter holes arranged in a hexagonal pattern. With the chamber exposed to cosmic rays, we observed that all the LEMs charge up in a relatively short period of less than a day. Once charged up, the LEMs can be operated at a stable gain of at least ~ 20 with none or very few discharges occurring across the electrodes. We have also shown that a uniform gain and excellent charge sharing can be achieved in our setup.

Our tests demonstrate that the LEM is a robust apparatus that is well-understood and well-suited for operation in ultra-pure cryogenic environments and that can maintain stable gains that match the goals of future large-scale liquid argon TPCs. In this context we are now in the process of manufacturing and testing LEMs and anodes with an active area of $50 \times 50 \text{ cm}^2$ which are soon to be operated on LAr LEM TPCs of much larger dimensions [9].

References

- [1] A. Badertscher *et al.*, “Construction and operation of a Double Phase LAr Large Electron Multiplier Time Projection Chamber,” [arXiv:0811.3384 [physics.ins-det]].
- [2] A. Badertscher, L. Knecht, M. Laffranchi, D. Lussi, A. Marchionni, G. Natterer, P. Otiougova and F. Resnati *et al.*, “Operation of a double-phase pure argon Large Electron Multiplier Time Projection Chamber: Comparison of single and double phase operation,” Nucl. Instrum. Meth. A **617**, 188 (2010) [arXiv:0907.2944 [physics.ins-det]].
- [3] A. Badertscher *et al.*, “First operation of a double phase LAr Large Electron Multiplier Time Projection Chamber with a 2D projective readout anode” Nucl. Instrum. Meth. A **641**, 48-57 (2011).
- [4] S. Amerio *et al.* [ICARUS Collaboration], “Design, construction and tests of the ICARUS T600 detector,” Nucl. Instrum. Meth. A **527**, 329 (2004).
- [5] A. Rubbia, “Experiments for CP violation: A Giant liquid argon scintillation, Cerenkov and charge imaging experiment?,” [hep-ph/0402110].
- [6] A. Rubbia, “Underground Neutrino Detectors for Particle and Astroparticle Science: The Giant Liquid Argon Charge Imaging Experiment (GLACIER),” J. Phys. Conf. Ser. **171**, 012020 (2009). [arXiv:0908.1286 [hep-ph]].
- [7] A. Badertscher *et al.*, “Giant Liquid Argon Observatory for Proton Decay, Neutrino Astrophysics and CP-violation in the Lepton Sector (GLACIER),” [arXiv:1001.0076 [physics.ins-det]].
- [8] A. Stahl, C. Wiebusch, A. M. Guler, M. Kamiscioglu, R. Sever, A. U. Yilmazer, C. Gunes and D. Yilmaz *et al.*, “Expression of Interest for a very long baseline neutrino oscillation experiment (LBNO),” CERN-SPSC-2012-021.
- [9] L. Agostino *et al.*, “LBNO-DEMO: Large-scale neutrino detector demonstrators for phased performance assessment in view of a long-baseline oscillation experiment,” arXiv:1409.4405 [physics.ins-det]. CERN-SPSC-2014-013. SPSC-TDR-004 (April 2014).
- [10] A. Bondar *et al.*, “Thick GEM versus thin GEM in two-phase argon avalanche detectors,” JINST **3**, P07001 (2008) [arXiv:0805.2018 [physics.ins-det]].
- [11] A. Badertscher *et al.*, “Stable operation with gain of a double phase Liquid Argon LEM-TPC with a 1 mm thick segmented LEM,” J. Phys. Conf. Ser. **308** (2011) 012016. [arXiv:1010.2482 [physics.ins-det]].

- [12] A. Badertscher, A. Curioni, U. Degunda, L. Epprecht, A. Gendotti, S. Horikawa, L. Knecht and D. Lussi *et al.*, “First operation and performance of a 200 lt double phase LAr LEM-TPC with a 40x76 cm² readout,” JINST **8**, P04012 (2013) [arXiv:1301.4817 [physics.ins-det]].
- [13] C. Cantini *et al.* “Long-term operation of a double phase LAr LEM Time Projection Chamber with a simplified anode and extraction-grid design,” JINST **9**, P03017 (2014) [arXiv:1312.6487 [physics.ins-det]].
- [14] K. Mavrokoridis *et al.* “Optical Readout of a Two Phase Liquid Argon TPC using CCD Camera and THGEMs” JINST **9**, P02006 (2014) [arXiv:1401.0525 [physics.ins-det]].
- [15] Breskin, A. *et al.* “A Concise review on THGEM detectors” Nucl. Instrum. Meth. **A598**, 107-111 (2009). [arXiv:0807.2026 [physics.ins-det]].
- [16] T. Aoyama, “Generalized Gas Gain Formula for Proportional Counters”, Nucl. Instrum. Meth. **A234**, 125 (1985).
- [17] R. Veenhof., “Magboltz - transport of electrons in gas mixtures”, version 8.9, <http://consult.cern.ch/writeup/magboltz/>
- [18] F. Resnati, “Modeling, design and first operation of the novel double phase LAr LEM-TPC detector”, PhD thesis, ETH Zurich (2012)
- [19] J. Rico, “First study of the stopping Muon sample with the ICARUS T600 detector,” Ph.D. Dissertation, ETH 14906 (2002)
- [20] D. Lussi, “Study of the response of the novel LAr LEM-TPC detector exposed to cosmic rays and a charged particle beam”, PhD thesis, ETH Zurich (2013)
- [21] S. Amoruso *et al.* [ICARUS Collaboration], “Study of electron recombination in liquid argon with the ICARUS TPC,” Nucl. Instrum. Meth. A **523**, 275 (2004).
- [22] M. Alfonsi *et al.* “Simulation of the dielectric charging-up effect in a GEM detector.” Nucl. Instrum. Meth. A **671**, 6 (2012).
- [23] M. Alexeev *et al.* “The quest for a third generation of gaseous photon detectors for Cherenkov imaging counters.” Nucl. Instrum. Meth. A **610**, 174 (2009).